Proceedings of the ASME 2018 International Design Engineering Technical Conferences & Computers and Information in Engineering Conference
IDETC/CIE 2018
August 26-29, 2018, Quebec City, Canada

DETC2018-85993

EFFECTS OF SQUEEZE FILM AND INITIAL DEFLECTION ON THE RESONANCE FREQUENCIES AND MODAL DAMPING OF CIRCULAR MICROPLATES

Aymen Jallouli[1], Najib Kacem[1,*], Fehmi Najar[2] and Joseph Lardies[1]
[1]Univ. Bourgogne Franche-Comté, FEMTO-ST Institute, CNRS/UFC/ENSMM/UTBM,
Department of Applied Mechanics, Besançon, France 25000
[2]Applied Mechanics and Systems Research Laboratory, Tunisia Polytechnic School,
University of Carthage, B.P. 743, La Marsa, 2078, Tunisia
*Corresponding author: najib.kacem@femto-st.fr

ABSTRACT

We investigate the effects of squeeze air film and initial deflection on the resonance frequencies and modal damping of capacitive circular microplates. The equation of motion of a circular microplate, which are derived from the von kármán plate theory, coupled with the Reynolds equation are discretized using the Differential Quadrature Method (DQM). The eigenvalues and eigenvectors of the multiphysical problem are determined by perturbing the system of equations around a static solution. Therefore, the resonance frequencies, modal damping coefficients and mode shapes of the plate and the fluid can be determined. The advantage of using DQM is that the solution of the system can be obtained with only few grid points. The obtained numerical results are compared with the experimental data for the case of a capacitive circular microplates with an initial deflection. The increase of the static pressure leads to a shift in the resonance frequencies due to the increase in the stiffness of the plate. Also the initial deflection change the resonance frequencies due to the change in the effective gap distance. The developed model is an effective tool to predict the dynamic behavior of a microsystem under the effect of air film and with initial deflection.

INTRODUCTION

Capacitive resonators have been the subject of extensive research for the last decades. This interest has led to many applications such as MEMS accelerometers and gyroscopes [1–4], pressure sensor [5], mass sensors [6–8] and radio frequency antennas [9].

One of the most used actuators in MEMS is the ultrasonic transducer, which is used to generate ultrasonic waves by vibrating the surface of the mechanical structure at a high frequency. These microdevices have been used in several applications like medical imaging [10] and therapy [11].

Characterization of capacitive micromachined ultrasonic transducers (CMUTs) has two major problems: The first one is the imperfection produced from the fabrication method like residual stress and initial deflection. The second problem is the effect of the fluid between the two electrodes. The fluid film can change dramatically the dynamic behavior of capacitive resonators by adding a stiffness and damping to the system.

The effects of initial deflection have been investigated in several studies. Ouakad *et al*. [12] studied the effect of an initial deflection on the static response of a microbeam. They showed that an increase in the the downward initial deflection leads to a decrease in the pull-in voltage due to the fact that the microbeam becomes closer to the bottom electrode. However, The upward initial deflection results in a snap through behavior [13] where the initial deflection increases the snap through voltage and decreases the pull-in voltage.

For the case of microplates, Saghir *et al*. [14, 15] investigated the static and the dynamic behavior of a rectangular microplate with an initial deflection. Near primary resonance, the microplate has a hardening type behavior when the excitation

force is low and the increase in the AC voltage increases the gap between the two stable solutions. The dynamic behavior of the microresonator was also investigated at $\omega/3$ super-harmonic. In this case, the increase in the AC voltage does not only increase the vibration amplitude but also changes the nonlinear dynamic behavior from hardening to softening. Medina *et al*. [16, 17] developed a reduced order model for a circular capacitive microplate, which has been validated using finite element analysis. The analysis revealed that due to the nonlinearity of the electrostatic force, the snap-through occurs at a lower displacement compared to the one induced by mechanical loads.

One of the techniques that have been used to study the effect a surrounding fluid on microsystems is the finite element method (FEM). Chaterjee *et al*. [18] used the modal projection method implemented in ANSYS to determine the stiffness and modal damping coefficients of a cantilever. The effect of the DC voltage was investigated at different pressures and it was shown that the static pressure can shift the resonance frequency of microsystems and increases the damping forces. FEM models are very efficient especially for systems with complicated shapes like perforated plates [19,20]. However, this type of model is computationally very time consuming, making it difficult to use when a large number of simulations are needed.

In order to overcome these problems, Younis *et al*. [21] developed a reduced order model of a rectangular microplate under the effect of air film using the Galerkin method. The obtained system of differential equation is solved using the perturbation method to determine the displacement and the pressure distributions of flexible microstructures. The model is used to determine an analytical expression of the damping coefficient and the natural frequency of the coupled problem. The obtained results have been compared with the experimental tests and they were in a good agreement.

In this paper, we present a different technique that can be used to investigate the effect of surrounding fluid on the resonance frequencies of a circular microplate. The system of equations, which is composed of the mechanical equation of motion and Reynolds equation, is transformed into a set of ordinary differential equations using DQM. The eigenvalue problem is then solved by perturbing the system around the static solution. We proved that the static pressure in the gap can add stiffness and damping to the system. By comparing the resonance frequencies at vacuum and atmospheric condition, a shift of 60 % is occurred for the first mode, which proved the importance of taking into consideration the squeeze film effects during the modeling of such microsystem. Also, we showed that at atmospheric condition, the initial deflection changes the resonance frequency due to the change in the gap distance between the two electrodes.

MATHEMATICAL MODEL

Equations of Motion

In this section, we consider a circular microplate with a uniform cross-section h and a homogeneous material with a density ρ, a Young's modulus E, which is the equivalent Young's modulus of the plate with a multilayer materials, and a Poisson ratio ν, as shown in Figure 1. The vibrating electrode is modeled as a perfectly clamped circular microplate with radius R excited with an electric voltage $V(t) = V_{dc} + V_{ac}\ cos(\omega t)$, where V_{dc} is the static electric voltage and V_{ac} is the amplitude of the harmonic voltage. The bottom electrode, with radius R_e and thickness d_e, is placed below the microplate at a distance d. We suppose that the microplate is subjected to an axisymetric initial deflection $w_0(r)$ defined as follows:

$$w_0(r) = w_{\max} \cos\left(\frac{\pi r}{2R}\right) \tag{1}$$

where $w_{\max}$ represent the initial deflection of the membrane at its center. We chose this expression of the initial deflection because it satisfies the boundary conditions of a clamped circular microplate and also it is a good approximation for the initial deflection determined experimentally.

As we can see in Figure 2, the microplate has an upward initial deflection $w_{\max} = 270$ nm. The initial deflection of the membrane is due to two effects [22]: (i) The stress gradient, which is due to the deposition of a thin layer of Aluminum on the upper surface of the microplate, (ii) The deformation of the substrate due to the fabrication process of the CMUT based on the anodic bonding technique of a SOI wafer on a glass wafer [23]. Since the two wafers have a different coefficient of thermal expansion, the deformation of the substrate leads to a deformation of the microplate.

The change in the gap distance leads to a change in the fluid pressure between the two plates. Hence, the mechanical differential equations, describing the multiphysical problem, can be

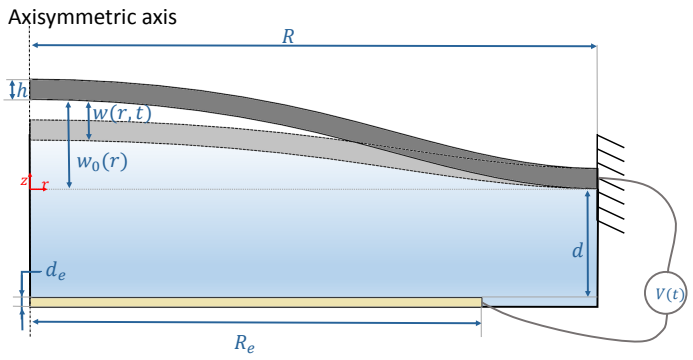

FIGURE 1: A schematic of a circular electrostatic thin microplate.

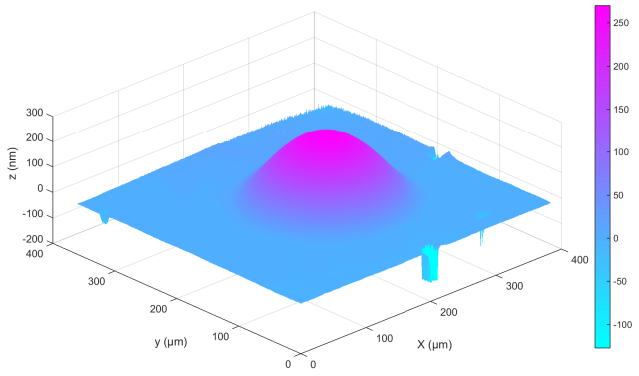

FIGURE 2: Topography of initial free shape of the microplate measured using interferometer.

written as:

$$\frac{\rho h^2}{D}\ddot{w}+\frac{h^2}{D}f_d+\nabla^4 w=\frac{N_0}{D}\left(\frac{1}{r}\left(w_{,r}+w_{0,r}\right)+\left(w_{,rr}+w_{0,rr}\right)\right)$$
$$+\frac{\varepsilon_0 V^2(t)}{2D(d-w+w_0)^2}-\frac{P(r,t)}{D}+\frac{12}{h^2}\left[\frac{1}{r}u_{,r}\left(w_{,r}+w_{0,r}\right)\right.$$
$$+u_{,rr}\left(w_{,r}+w_{0,r}\right)+u_{,r}\left(w_{,rr}+w_{0,rr}\right)+\frac{1}{2r}\left(w_{,r}\right)^2\left(w_{,r}+w_{0,r}\right)$$
$$+w_{,r}\left(w_{,r}+w_{0,r}\right)\left(\frac{1}{r}w_{0,r}+w_{0,rr}\right)+\frac{1}{2}\left(w_{,r}\right)^2\left(w_{,rr}+w_{0,rr}\right)$$
$$+w_{,r}w_{0,r}\left(w_{,rr}+w_{0,rr}\right)+w_{,rr}\left(w_{,r}+w_{0,r}\right)^2$$
$$\left.+\frac{\nu}{r}\left(u_{,r}\left(w_{,r}+w_{0,r}\right)+u\left(w_{,rr}+w_{0,rr}\right)\right)\right] \quad (2)$$

$$u_{,rr}+\frac{1}{r}u_{,r}-\frac{u}{r^2}=-\frac{1-\nu}{2r}\left(\left(w_{,r}\right)^2+2w_{,r}w_{0,r}\right)$$
$$-w_{,rr}\left(w_{,r}+w_{0,r}\right)-w_{,r}w_{0,rr} \quad (3)$$

where $u(r,t)$ and $w(r,t)$ are the in-plane and out-of-plane displacement of the plate, $P(r,t)$ represents the net pressure force applied on the lower surface of the plate, ∇^4 is the bi-harmonic operator expressed as $\nabla^4=\left(\frac{\partial^2}{\partial r^2}+\frac{1}{r}\frac{\partial}{\partial r}\right)^2$ and $D=\frac{Eh^3}{12\left(1-\nu^2\right)}$ is the plate flexural rigidity. f_d is the damping force. ε_0 the permittivity of the air. N_0 is the residual stress applied on the plate. Assuming axisymmetric pressure distribution, the pressure component is determined by solving the following Reynolds equation of a fluid between two circular plates:

$$\frac{\partial}{\partial r}\left(rH^3P_t\frac{\partial P_t}{\partial r}\right)=12\eta r\left(H\frac{\partial P_t}{\partial t}+P_t\frac{\partial H}{\partial t}\right) \quad (4)$$

where η is the viscosity coefficient of the fluid, H is the total gap distance between the two plates and P_t represents the total pressure in the gap, which are defined as:

$$P_t=P_0+P(t)$$
$$H=d_t(r)+w_0(r)-w(r,t) \quad \text{where} \quad d_t(r)=\begin{cases} d & r\le R_e \\ d+d_e & r>R_e \end{cases} \quad (5)$$

and P_0 is the local pressure of the medium. For the pressure boundary conditions, we suppose that the fluid is trapped inside the gap. Therefore, the flux at the clamped edge is equal to zero and at the center of the plate the pressure is maximum which means that the derivative of P_t with respect to r is zero. Hence, the boundary conditions of a circular plate are defined as:

$$\begin{array}{llll} \text{At } r=0: & w_{,r}=0 & u=0 & P_{,r}=0 \\ \text{At } r=R: & w_{,r}=w=0 & u=0 & P_{,r}=0 \end{array} \quad (6)$$

The Reynolds equation (4) is derived from the NavierStokes equation by approximating the gas in the gap to be continuum and this is depending on the value of the Knudsen number K_n defined as:

$$K_n=\frac{P_a\lambda_a}{P_0H} \quad (7)$$

where P_a and λ_a are the pressure and the molecular mean free path of the fluid at ambient condition. In general, there are four regimes of flow depending on the Knudsen number K_n: continuum regime ($K_n<0.001$), transition regime ($0.001\le K_n\le 0.1$), slip-flow regime ($0.1\le K_n\le 10$) and molecular regime ($K_n>10$). At the continuum flow the dynamic of the fluid is governed by the Reynolds equation (4). However, for a very small gap distance H and low pressure P_0, the flow becomes noncontinuous and the Reynolds equation becomes suspect to use. Several studies have been conducted to extend the validity domain of the Reynolds equation by introducing an effective viscosity coefficient η_{eff} which depends on the Knudsen number K_n. One of the most used models is the approximation of Veijola *et al*. [24] which is given by:

$$\eta_{eff}=\frac{\eta}{1+9.638K_n^{1.159}} \quad (8)$$

Nondimensional Equations of Motion

In order to reduce the number of physical parameters used in the simulation we define the following nondimensional variables:

$$\begin{aligned}
&\tilde{r} = Rr; && \tilde{u} = du; && \tilde{w} = dw \\
&\tilde{c} = \frac{(D\rho h)^{1/2}}{R^2}c; && \gamma = \frac{12Rd}{h^2}; && \beta = \frac{d}{R} \\
&\tilde{N}_0 = \frac{D}{R^2}N_0; && \tilde{t} = Tt = R^2\left(\frac{\rho h}{D}\right)^{1/2}t; && \alpha_e = \frac{\varepsilon_0 R^4}{2Dd^3} \\
&\tilde{P}_t = P_0 P_t = P_0(1+P); && \tilde{H} = dH && P_{ND} = \frac{R^4 P_0}{Dd};
\end{aligned} \tag{9}$$

Substituting (9) into (2-4) and dropping the tilde ($\sim$), we get:

$$\begin{aligned}
\ddot{w} + c\dot{w} + \nabla^4 w = N_0\left(\frac{1}{r}(w_{,r} + w_{0,r}) + (w_{,rr} + w_{0,rr})\right) \\
+ \alpha_e \frac{V^2(t)}{(1 - w + w_0)^2} - P_{ND}P + \gamma\hat{\Gamma}(w, u, w_0)
\end{aligned} \tag{10}$$

$$\begin{aligned}
u_{,rr} + \frac{1}{r}u_{,r} - \frac{u}{r^2} = -\frac{1-\nu}{2r}\left((w_{,r})^2 + 2w_{,r}w_{0,r}\right) \\
- w_{,rr}(w_{,r} + w_{0,r}) - w_{,r}w_{0,rr}
\end{aligned} \tag{11}$$

$$\frac{\partial}{\partial r}\left(rH^3 P_t \frac{\partial P_t}{\partial r}\right) = \sigma r\left(H\frac{\partial P_t}{\partial t} + P_t\frac{\partial H}{\partial t}\right) \tag{12}$$

where $\hat{\Gamma}$ is defined as:

$$\begin{aligned}
\hat{\Gamma}(w, u, w_0) = \frac{1}{r}u_{,r}(w_{,r} + w_{0,r}) + u_{,rr}(w_{,r} + w_{0,r}) + u_{,r}(w_{,rr} + w_{0,rr}) \\
+ \beta\left(\frac{1}{2r}(w_{,r})^2(w_{,r} + w_{0,r}) + w_{,rr}(w_{,r} + w_{0,r})^2\right. \\
+ w_{,r}(w_{,r} + w_{0,r})\left(\frac{1}{r}w_{0,r} + w_{0,rr}\right) + \frac{1}{2}(w_{,r})^2(w_{,rr} + w_{0,rr}) \\
\left. + w_{,r}w_{0,r}(w_{,rr} + w_{0,rr})\right) + \frac{\nu}{r}\left(u_{,r}(w_{,r} + w_{0,r}) + u(w_{,rr} + w_{0,rr})\right)
\end{aligned} \tag{13}$$

$\sigma = \frac{12\eta_{eff}R^2}{d^2 P_0 T}$ represents the squeeze number [25], which refers to the compressibility of the fluid in the gap.

The nondimensional boundary conditions (6) are transformed to:

$$\begin{aligned}
&\text{At } r = 0: && w_{,r} = 0 && u = 0 && P_{,r} = 0 \\
&\text{At } r = 1: && w_{,r} = w = 0 && u = 0 && P_{,r} = 0
\end{aligned} \tag{14}$$

Discretization of the Equations of Motion

To solve the multiphysical problem, we use the DQM. The derivative of the unknown parameters w, u and P can be expressed as:

$$\begin{aligned}
&\left[\frac{\partial^k w}{\partial r^k}\right]_{r=r_i} = \sum_{j=1}^{n} A_{ij}^{(k)} w_j; \qquad \left[\frac{\partial^k u}{\partial r^k}\right]_{r=r_i} = \sum_{j=1}^{n} A_{ij}^{(k)} u_j; \\
&\left[\frac{\partial^k P}{\partial r^k}\right]_{r=r_i} = \sum_{j=1}^{n} A_{ij}^{(k)} P_j
\end{aligned} \tag{15}$$

where w_j, u_j and P_j are respectively the radial displacement, transverse displacement and the net pressure at the grid point $r = r_i$, defined by Chebyshev-Gauss-Lobatto [26]:

$$r_i = \frac{1}{2}\left(1 - \cos\left(\frac{(i-1)}{(n-1)}\pi\right)\right) \tag{16}$$

w_i, u_i are the radial and transverse displacements of plate at the grid point $r = r_i$. $A_{ij}^{(k)}$ are the DQM weighting coefficients of the kth order derivative which defined in [27].

Therefore, the discretized form of the microplate equations coupled with the Reynolds equation can be written as:

$$\begin{aligned}
&\ddot{w}_i + c\dot{w}_i + \nabla^4 w_i = \\
&N_0\left(\frac{1}{r_i}\left(\sum_{j=1}^{n} A_{ij}^{(1)} w_j + w_{0,r}^i\right) + \left(\sum_{j=1}^{n} A_{ij}^{(2)} w_j + w_{0,rr}^i\right)\right) \\
&+ \alpha_e \frac{V^2(t)}{\left(1 - w_i + w_0^i\right)^2} - P_{ND}P_i + \gamma\hat{\Gamma}_i\left(w_j, u_j, w_0^i\right);\ i = 2, \cdots, n-2
\end{aligned} \tag{17}$$

$$\sum_{j=1}^{n} A_{ij}^{(2)} u_j + \frac{1}{r_i}\sum_{j=1}^{n} A_{ij}^{(1)} u_j - \frac{u_i}{r_i^2} = -\beta\left(\frac{1-\nu}{2r_i}\left(\left(\sum_{j=1}^{n} A_{ij}^{(1)} w_j\right)^2 + 2w_{0,r}^{i}\sum_{j=1}^{n} A_{ij}^{(1)} w_j\right) + \sum_{j=1}^{n} A_{ij}^{(2)} w_j\left(\sum_{j=1}^{n} A_{ij}^{(1)} w_j + w_{0,r}^{i}\right) + w_{0,rr}^{i}\sum_{j=1}^{n} A_{ij}^{(1)} w_j\right); \quad i = 2,\cdots,n-1 \tag{18}$$

$$\sum_{j=1}^{n} A_{ij}^{(1)}\left(r_j H_j^3 (1+P_j)\sum_{k=1}^{n} A_{jk}^{(1)} P_k\right) = \sigma r_i\left(H_i\dot{P}_i - (1+P_i)\dot{w}_i\right); \quad i = 2,\cdots,n-1 \tag{19}$$

where $\hat{\Gamma}_i$ is the discretized form of $\hat{\Gamma}$ defined in equation (13), H_i is the nondimensional film thickness at the i^{th} grid point defined as:

$$H_i = d_t(r_i) + w_0(r_i) - w_i(t) \quad \text{where} \quad d_t(r_i) = \begin{cases} 1 & r_i \le \frac{R_e}{R} \\ 1 + \frac{d_e}{d} & r_i > \frac{R_e}{R} \end{cases} \tag{20}$$

and the boundary conditions are :

$$\begin{aligned} &\text{At } r=0: \quad \sum_{j=1}^{n} A_{1j}^{(1)} w_j = 0 \qquad u_1 = 0 \quad \sum_{j=1}^{n} A_{1j}^{(1)} \bar{P}_j = 0 \\ &\text{At } r=1: \quad \sum_{j=1}^{n} A_{nj}^{(1)} w_j = w_n = 0 \quad u_n = 0 \quad \sum_{j=1}^{n} A_{nj}^{(1)} \bar{P}_j = 0 \end{aligned} \tag{21}$$

EIGENVALUE ANALYSIS

In this section, we investigate the eigenvalue problem of the microplate under the effect of the squeeze film The system of equation (17)-(19) is composed of three equation: The first equation (17), which describe the dynamic behavior of the plate, a system of ordinary differential equations with a size $n-3$. The second equation (18) is an algebraic equation that represent the in-plane displacement u as function of the out-of-plane displacement w. The third equation (18) is the Reynolds equation that couple the displacement w with the pressure in the gap P.For n grid points the total number of equations is equal to $3 \times n$ which makes the computational time huge. To reduce the number of equations, we write the radial displacement u_i as a function of w_i using equation (18). At the boundary nodes, we use the boundary equations (21) to determine the boundary displacement $\{w_1, w_{n-1}, w_n\}$ and pressure $\{P_1, P_n\}$. This simplification reduces the total number of equations to $(n-3)\times(n-2)$.Next, we decompose the total displacement w_i into a static component w_i^s and dynamic component w_i^d.

$$w(r = r_i, t) = w_i(t) = w_i^s + w_i^d(t) \tag{22}$$

Therefore the system of equation (17) and (19) can be written as:

$$M\ddot{Y}(t) + C\dot{Y}(t) + KY(t) + K_{NL}(Y(t), \dot{Y}(t)) = 0 \tag{23}$$

where M, C and K are the mass, damping and stiffness matrices; $K_{NL}(Y(t), \dot{Y}(t))$ is the vector with nonlinear parameters and $Y(t)$ is the vector of unknowns defined as:

$$Y(t) = \left\{w_2^d, \cdots, w_{n-2}^d, P_2, \cdots, P_{n-1}\right\} \tag{24}$$

To determine the resonance frequencies and damping coefficients, we neglect the nonlinear part K_{NL}. Even with this approximation, the solving of this type of system (23) remains difficult. Therefore, we follow the work of Meirovitch *et al*. [28] and we transform equation (23) to the general eigenvalue problem by defining $\chi_1 = Y(t)$ and $\chi_2 = \dot{Y}(t)$:

$$\begin{bmatrix} M & 0 \\ 0 & -K \end{bmatrix} \frac{\partial}{\partial t}\begin{bmatrix} \dot{Y} \\ Y \end{bmatrix} = \begin{bmatrix} -C & -K \\ -K & 0 \end{bmatrix}\begin{bmatrix} \dot{Y} \\ Y \end{bmatrix} \tag{25}$$

Next, we determine the linear damped eigenvalues and eigenvectors by formulating the harmonic displacement amplitude and pressure as follow:

$$\begin{aligned} w_i^d(t) &= \phi_i e^{j\omega t} \\ P_i(t) &= \varphi_i e^{j\omega t} \end{aligned} \tag{26}$$

where ϕ_i and φ_i are the shape functions of the microplate and fluid pressure associated to the frequency ω at the nodes $r = r_i$. Substituting the expression of w_i and P_i into equation (25), the system of equations becomes:

$$(\lambda A - B)\chi = 0 \tag{27}$$

where

$$\lambda = j\omega \qquad A = \begin{bmatrix} M & 0 \\ 0 & -K \end{bmatrix} \qquad B = \begin{bmatrix} -C & -K \\ -K & 0 \end{bmatrix}$$

$$\chi = \{\lambda Y, Y\} = \Big\{\lambda\phi_2^d, \cdots, \lambda\phi_{n-2}^d, \lambda\varphi_2, \cdots, \lambda\varphi_{n-1}, \phi_2^d, \cdots, \phi_{n-2}^d, \varphi_2, \cdots, \varphi_{n-1}\Big\} \quad (28)$$

The eigenvalues and eigenvectors are then obtained by solving equation (27). The resonance frequency and the damping parameter of the ith mode satisfy:

$$\omega_i = |\mathrm{Re}\,(-j\lambda_i)| \qquad \text{and} \qquad \xi_i = \frac{|\mathrm{Im}\,(-j\lambda_i)|}{|\mathrm{Re}\,(-j\lambda_i)|} \quad (29)$$

where Re and Im denote the real and imaginary part, respectively.

RESULTS AND DISCUSSION

Convergence of the Solution

As a first step, it is important to check the convergence of the DQM solution with respect to the number of grid points. In figure 3, we determined the first two resonance frequencies of the microplate for different number of points n. For these simulations, we used the physical parameters of the solid and fluid presented in Table 1, where the residual stress N_0 is determined in order to mach the numerical and experimental first two resonance frequencies [15].

TABLE 1: Physical parameters of the CMUT

Symbol	Quantity	Dimension
E	Youngs modulus	149 [GPa]
ρ	Density	2330 [kg/m^3]
ν	Poisson's ratio	0.27
R	Radius of the microplate	116 [μm]
R_e	Radius of the electrode	75 [μm]
h	Thickness of the microplate	2.25 [μm]
d	Gap distance	0.77 [μm]
d_e	Thickness of the electrode	0.3 [μm]
ε_0	Permittivity of the air	8.85 10^{-12} [F/m]
N_0	Residual stress	2.5 [MPa]
η	Viscosity	1.83 10^{-5} [Ns/m^2]
λ_a	Atmospheric mean free path	64 [nm]

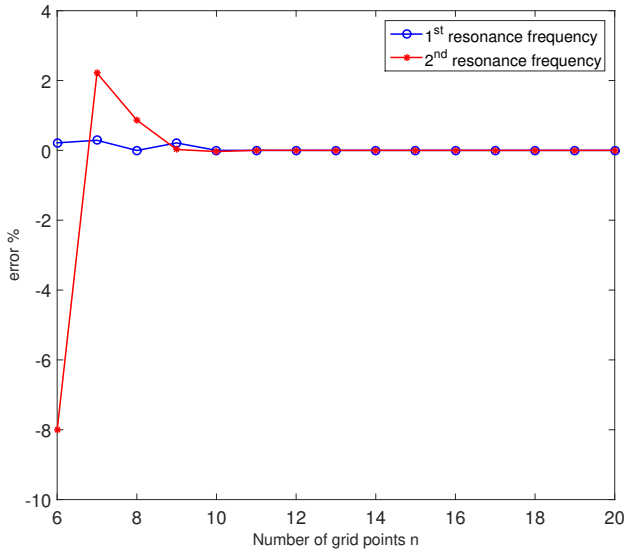

FIGURE 3: The convergence of the first two resonance frequencies for a pressure $P_0 = 1$ atm with respect to the case when $n = 20$

The resonance frequencies of the coupled system are determined for a clamped circular microplate at atmospheric conditions. With only $n = 6$ grid points, we can determine the first two resonance frequencies of the coupled problem with an error of 8 % for the 2^{nd} mode. By increasing the number of grid points, the three modes converge and 10 points are sufficient to investigate the eigenvalues of the coupled problem. The error of the first two resonance frequencies is less than 0.04 % and the computational time is about few seconds. The DQM is able to predict the first resonance frequencies of the coupled multiphysical system with only few grid points and a high accuracy.

Experimental validation

The resonance frequencies and mode shapes of a circular microplate are determined with the Micro System Analyzer (MSA-500) of *Polytec* industry. This vibrometer is mounted with scanning mirrors that can help to measure the displacement/velocity at a grid of points on the moving surface. Also it is equipped with a decoder with different precisions (can go up to 1 pm for the displacement and 10 m/s for the velocity) and wide frequency range (up to 24 MHz). The data acquisition is done with a MSA processing unit equipped with software to display frequency-domain and time-domain data and simplifies the transient response analysis. As we can see in Figure 4, we placed our wafer into a vacuum chamber in order to eliminate the fluid interaction with the microsystem. Two probes are placed inside the chamber to insure the electric connections. The vacuum chamber has a trans-

parent window (Plexiglas) that enables the laser beam to penetrate without any distortion. The DC voltage is generated with a DC generator and the harmonic voltage V_{ac} is generated with the MSA electrical generator. The two voltages are combined using a coupling circuit.

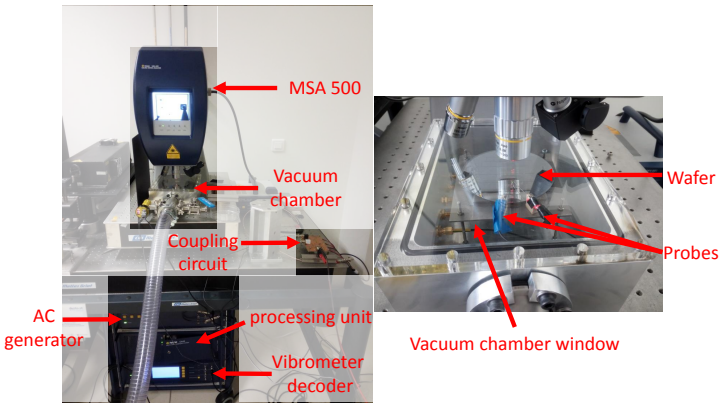

FIGURE 4: MSA-500 vibrometer used for resonance frequencies and mode shape measurements

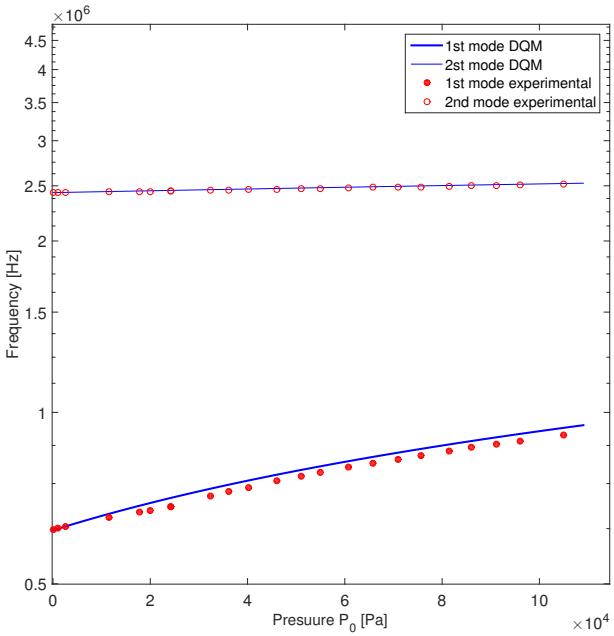

FIGURE 5: Experimental validation of the effect of the pressure in the gap on the resonance frequencies of a deflected microplate with initial deflection $w_{max} = 270$ nm

In Figure 5, we compare the experimental and numerical resonance frequencies of the microplate at different pressures P_0 by applying only a small AC voltage. For low pressure ($P_0 = 0.45$ mbar), the resonance frequencies of the microstructure are equal to the natural resonance frequencies of the microplate. At this pressure, the air effects on the solid are negligible. By increasing the pressure, the trapped air inside the gap behaves like a spring which explains the increase in the resonance frequencies. At $P_0 = 0.45$ mbar, the first resonance frequency is equal to $f_1 = 608$ kHz, which is equal to the natural resonance frequency of the system without air effects. However, for atmospheric conditions the resonance frequency increases up to $f_1 = 973$ kHz. The difference in the resonance frequency (60 % shift for the 1st resonance frequency) shows the importance of taking into consideration the squeeze film effects during the modeling of microsystems. The numerical simulations of a circular microplate with an initial deflection show a good agreement with the experimental results even when the squeeze forces are important. The maximum error between the experimental and numerical results is less than 2.5 %. This error can be explained by the imperfect boundary conditions of the plate due to the opening in the pad access.

The effect of an initial deflection on the eigenvalue problem

In Figure 6, we present the effect of the initial deflection on the first two resonance frequencies and damping parameters. The negative initial deflection leads to a decrease in the effective gap distance which is defined as [29]:

$$d_{eff}^2 \approx \frac{1}{R_e} \int_0^{R_e} (d + w_0(r))^2 dr \tag{30}$$

and when the two electrodes become closer, the trapped air in the gap behave as a spring which explains the shift in the resonance frequencies. However for a positive initial deflection, the effective gap distance increases which explains the increase in the damping forces and the decrease in effective stiffness.

Another major effect that is commonly studied in CMUTs is the DC voltage effects. The electrostatic force has a direct effect on the resonance frequencies. Figure 7 shows the variation of the first resonance frequency for the case of flat and deflected plate. As we increase the DC voltage, the fundamental natural frequency decreases until it drops to zero at a $V_{dc} = 34$ V for the case of flat plate and at a $V_{dc} = 52$ V for the case of deflected plate, also known as the pull-in voltage. The decrease in the resonance frequency is due to the negative stiffness caused by the electrostatic forces and at pull-in voltage, the electrostatic force is equal to the restoring forces of the microplate. The shift

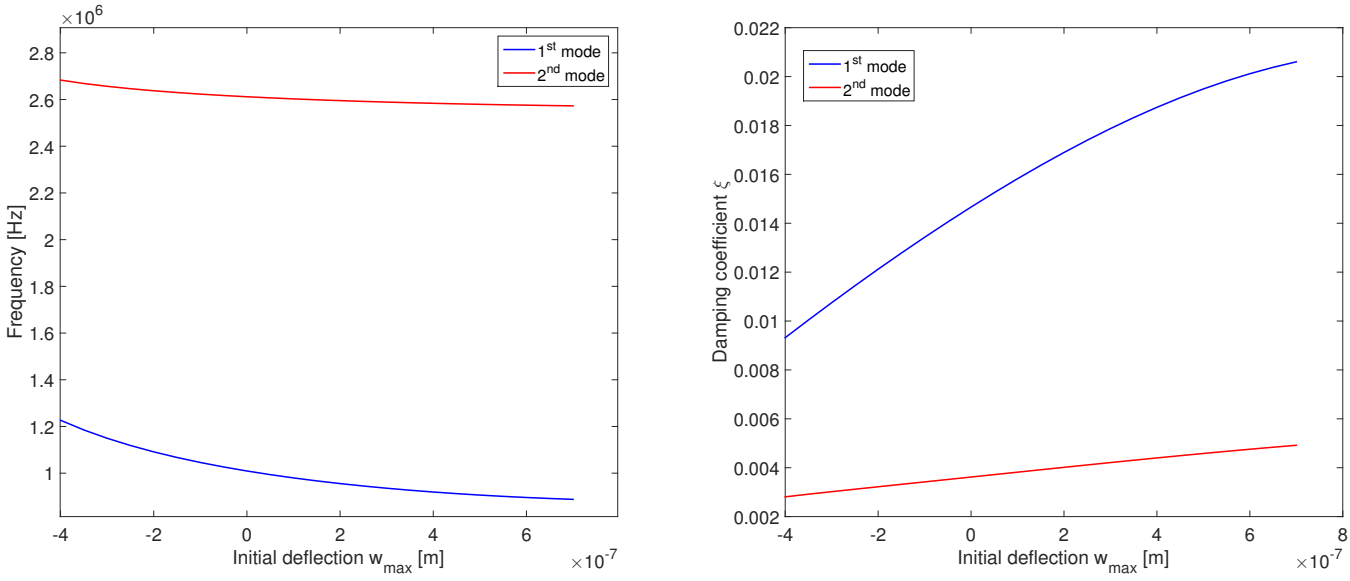

(a) (b)

FIGURE 6: The effect of changing the plate initial deflection w_{max} on the resonance frequencies and damping coefficients for the first two axisymmetric modes at atmospheric condition.

in the pull-in voltage between the flat and deflected membrane is due to the increase in the effective gap distance. By increasing the static pressure, the difference between the two cases (flat and deflected) increases due to the difference in the gap distance.

The mode shapes of the coupled problem

One of the most important features of the differential quadrature method is the possibility to determine the mode shapes for both the microplate and the fluid. In Figure 8, we present the real and the imaginary eigenvectors of w and P at atmospheric condition for the microplate with an initial deflection $w_{max} = 270$ nm. For the case of the displacement w, the mode shapes satisfy the boundary and axisymmetric conditions (horizontal tangent at $r = 0$ and $r = 1$ and $w(1) = 0$). For the case of the fluid, the mode shapes satisfy the following boundary conditions: zero flux at $r = 0$ and $r = 1$. For $r = R_e/R = 0.65$, we can see the change in the slope of the mode shape of the fluid and this is due to the increase in the gap distance:

$$d_t(r_i) = \begin{cases} 1 & r_i \leq \frac{R_e}{R} \\ 1 + \frac{d_e}{d} & r_i > \frac{R_e}{R} \end{cases} \tag{31}$$

For this case, the change in the gap distance and initial deflection can be easily taken into consideration when we use the differential quadrature method.

CONCLUSION

In this paper, we presented a mathematical model of a capacitive circular microplate with an initial deflection and in interaction with an air film. The mechanical equations of motion coupled with the Reynolds equation have been solved using DQM. This method is fast and efficient for a multiphysical problem, since it converges for a low number of grid points. The presented model is then validated with respect to experimental results for different static pressures. In vacuum condition, the resonance frequencies of the multiphysical system and the microplate are equal and the increase in the static pressure leads to an increase in the resonance frequencies. Moreover, the increase in the initial deflection leads to a decrease in the effective stiffness and an increase in the damping coefficients, which is due to the change in the effective gap distance.

REFERENCES

[1] Devices, A., 1996. "Adxl50 monolithic accelerometer with signal conditioning". *Data sheet*.

[2] Boxenhorn, B., and Greiff, P., 1988. "A vibratory micromechanical gyroscope". In Guidance, Navigation and Control Conference, p. 4177.

[3] Kacem, N., Hentz, S., Pinto, D., Reig, B., and Nguyen, V., 2009. "Nonlinear dynamics of nanomechanical beam resonators: improving the performance of nems-based sensors". *Nanotechnology,* ***20***(27), p. 275501.

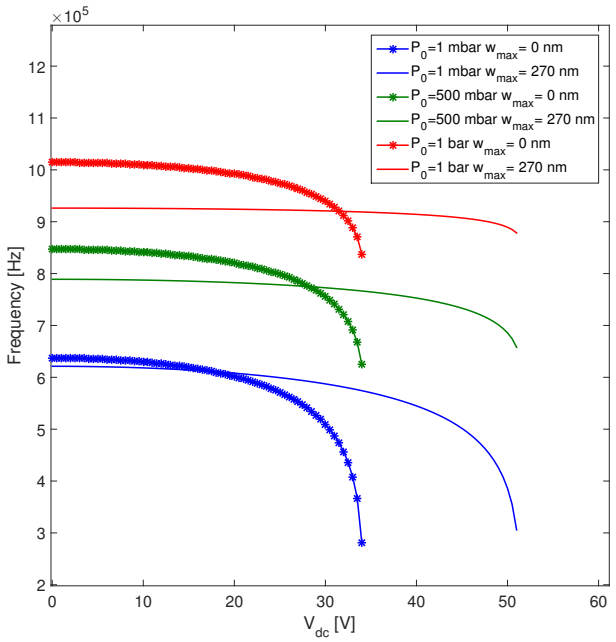

FIGURE 7: The effect of changing V_{dc} on the first resonance frequency of a flat and deflected microplate

[4] Kacem, N., Hentz, S., Baguet, S., and Dufour, R., 2011. "Forced large amplitude periodic vibrations of non-linear mathieu resonators for microgyroscope applications". *International Journal of Non-Linear Mechanics,* ***46***(10), pp. 1347 – 1355.

[5] Eaton, W. P., and Smith, J. H., 1997. "Micromachined pressure sensors: review and recent developments". *Smart Materials and Structures,* ***6***(5), p. 530.

[6] Chaste, J., Eichler, A., Moser, J., Ceballos, G., Rurali, R., and Bachtold, A., 2012. "A nanomechanical mass sensor with yoctogram resolution". *Nature nanotechnology,* ***7***(5), pp. 301–304.

[7] Kacem, N., Arcamone, J., Perez-Murano, F., and Hentz, S., 2010. "Dynamic range enhancement of nonlinear nanomechanical resonant cantilevers for highly sensitive nems gas/mass sensor applications". *Journal of Micromechanics and Microengineering,* ***20***(4), p. 045023.

[8] Kacem, N., Baguet, S., Duraffourg, L., Jourdan, G., Dufour, R., and Hentz, S., 2015. "Overcoming limitations of nanomechanical resonators with simultaneous resonances". *Applied Physics Letters,* ***107***, p. 073105.

[9] Anagnostou, D. E., Zheng, G., Chryssomallis, M. T., Lyke, J. C., Ponchak, G. E., Papapolymerou, J., and Christodoulou, C. G., 2006. "Design, fabrication, and measurements of an rf-mems-based self-similar reconfigurable antenna". *IEEE Transactions on Antennas and Propagation,* ***54***(2), pp. 422–432.

[10] Khuri-Yakub, B. T., and Oralkan, Ö., 2011. "Capacitive micromachined ultrasonic transducers for medical imaging and therapy". *Journal of micromechanics and microengineering,* ***21***(5), p. 054004.

[11] Wong, S. H., Kupnik, M., Watkins, R. D., Butts-Pauly, K., and Khuri-Yakub, B. T., 2010. "Capacitive micromachined ultrasonic transducers for therapeutic ultrasound applications". *IEEE transactions on Biomedical Engineering,* ***57***(1), pp. 114–123.

[12] Ouakad, H. M., Najar, F., and Hattab, O., 2013. "Nonlinear analysis of electrically actuated carbon nanotube resonator using a novel discretization technique". *Mathematical Problems in Engineering,* ***2013***.

[13] Zhang, Y., Wang, Y., Li, Z., Huang, Y., and Li, D., 2007. "Snap-through and pull-in instabilities of an arch-shaped beam under an electrostatic loading". *Journal of Microelectromechanical Systems,* ***16***(3), pp. 684–693.

[14] Saghir, S., Bellaredj, M., Ramini, A., and Younis, M. I., 2016. "Initially curved microplates under electrostatic actuation: theory and experiment". *Journal of Micromechanics and Microengineering,* ***26***(9), p. 095004.

[15] Saghir, S., Ilyas, S., Jaber, N., and Younis, M. I., 2017. "An experimental and theoretical investigation of the mechanical behavior of multilayer initially curved microplates under electrostatic actuation". *Journal of Vibration and Acoustics,* ***139***(4), p. 040901.

[16] Medina, L., Gilat, R., and Krylov, S., 2016. "Bistable behavior of electrostatically actuated initially curved micro plate". *Sensors and Actuators A: Physical,* ***248***, pp. 193–198.

[17] Medina, L., Gilat, R., and Krylov, S., 2017. "Modeling strategies of electrostatically actuated initially curved bistable micro plates". *International Journal of Solids and Structures*.

[18] Chaterjee, S., and Pohit, G., 2010. "Squeeze-film damping characteristics of cantilever microresonators for higher modes of flexural vibration". *International Journal of Engineering, Science and Technology,* ***2***(4), pp. 187–199.

[19] Veijola, T., and Mattila, T., 2001. "Compact squeezed-film damping model for perforated surface". In *Transducers 01 Eurosensors XV*. Springer, pp. 1478–1481.

[20] Ishfaque, A., and Kim, B., 2017. "Analytical solution for squeeze film damping of mems perforated circular plates using greens function". *Nonlinear Dynamics,* ***87***(3), pp. 1603–1616.

[21] Nayfeh, A. H., and Younis, M. I., 2003. "A new approach to the modeling and simulation of flexible microstructures under the effect of squeeze-film damping". *Journal of Micromechanics and Microengineering,* ***14***(2), p. 170.

[22] Younis, M. I., 2011. Mems linear and nonlinear statics and

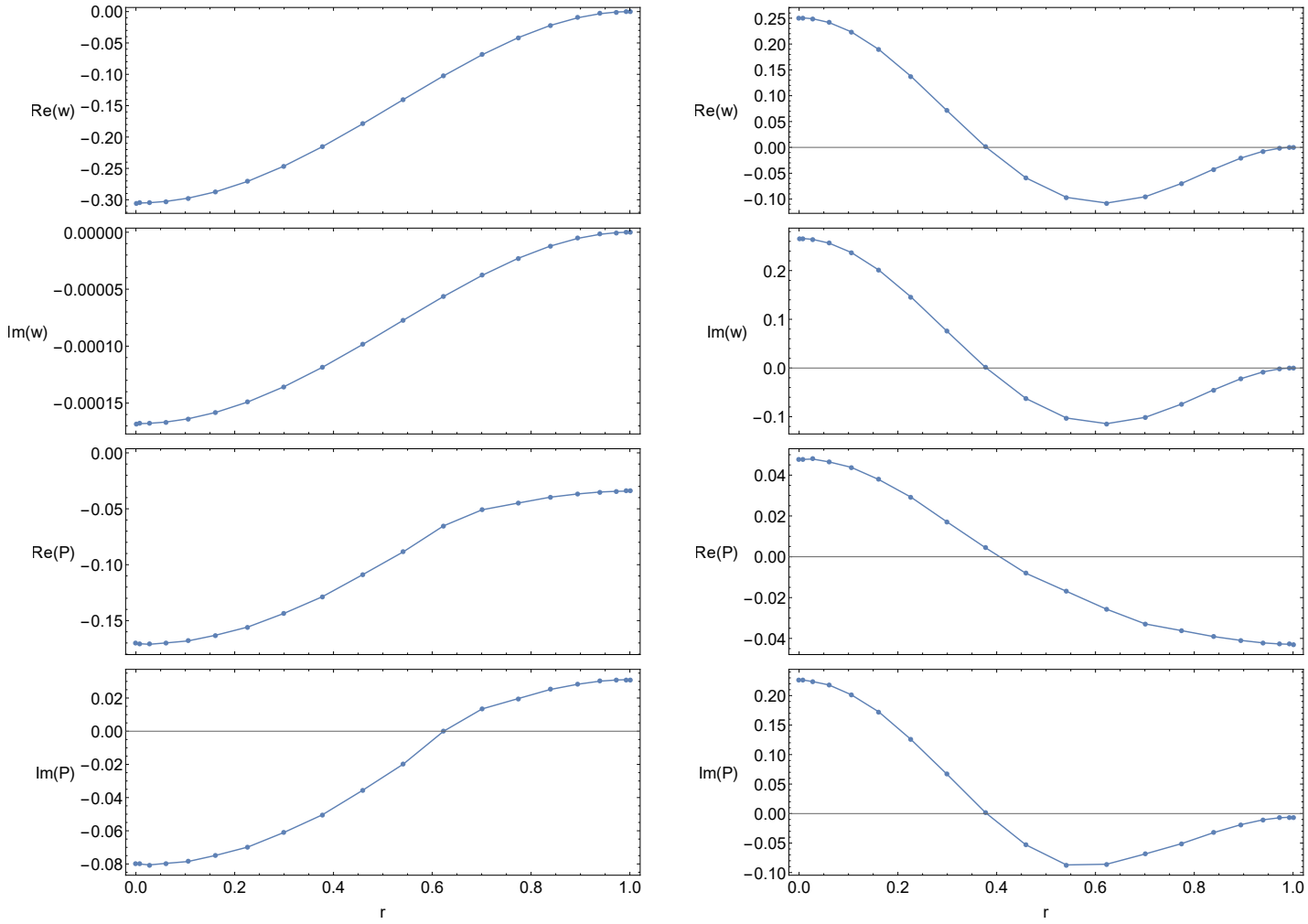

FIGURE 8: The real and imaginary eigenvectors of the first two axisymmetric modes ((a) the first mode and (b) the second mode) for the solid and fluid at atmospheric pressure $P_0 = 1$ atm and for 25 grid points

dynamics.

[23] Bellaredj, M., Bourbon, G., Walter, V., Le Moal, P., and Berthillier, M., 2014. "Anodic bonding using soi wafer for fabrication of capacitive micromachined ultrasonic transducers". *Journal of Micromechanics and Microengineering,* ***24***(2), p. 025009.

[24] Veijola, T., Kuisma, H., Lahdenperä, J., and Ryhänen, T., 1995. "Equivalent-circuit model of the squeezed gas film in a silicon accelerometer". *Sensors and Actuators A: Physical,* ***48***(3), pp. 239–248.

[25] Senturia, S. D., 2007. *Microsystem design*. Springer Science & Business Media.

[26] Bert, C. W., and Malik, M., 1996. "Semianalytical differential quadrature solution for free vibration analysis of rectangular plates". *AIAA journal,* ***34***(3), pp. 601–606.

[27] Quan, J., and Chang, C., 1989. "New insights in solving distributed system equations by the quadrature methodi. analysis". *Computers & Chemical Engineering,* ***13***(7), pp. 779–788.

[28] Meirovitch, L., 1980. *Computational methods in structural dynamics*, Vol. 5. Springer Science & Business Media.

[29] Jallouli, A., Kacem, N., Bourbon, G., Le Moal, P., Walter, V., and Lardies, J., 2016. "Pull-in instability tuning in imperfect nonlinear circular microplates under electrostatic actuation". *Physics Letters A,* ***380***(46), pp. 3886–3890.